Title: Effects of Frameworks and Mesoporosities on the Catalytic Activity of Hierarchical Zeolite Catalysts in Benzyl Alcohol Conversion

Authors: CHAO LI; Hong Je Cho; Zhuopeng Wang; Jinsheng Gou; Yanqun Ren; Hongxia Xi; Wei Fan

To be cited as: 10.1002/cctc.201600322

Link to VoR: http://dx.doi.org/10.1002/cctc.201600322

Effects of Frameworks and Mesoporosities on the Catalytic Activity of Hierarchical Zeolite Catalysts in Benzyl Alcohol Conversion

Chao Li,[a,b] Hong Je Cho,[b] Zhuopeng Wang, [b,c] Jinsheng Gou, [b,d] Yanqun Ren,[a] Hongxia Xi, *[a] and Wei Fan*[b]

The catalytic performance of 3 dimensionally ordered mesoporous imprinted (3DOm-i) zeolite catalysts with different frameworks (3DOm-i MFI, 3DOm-i BEA and 3DOm-i LTA) were investigated by liquid phase catalytic conversion of benzyl alcohol in mesitylene, and compared to other microporous and mesoporous catalysts with a high external surface area including MCM-22, 300 nm MFI, ITQ-2 and Al-MCM-41. The mesoporosity in MFI and BEA zeolites can effectively enhance the catalytic performance of the zeolite catalysts for the benzyl alcohol self-etherification catalyzed by both the acid sites on the external and internal surface, and the alkylation of mesitylene with benzyl alcohol exclusively catalyzed by the acid sites on the external surface. For the 3DOm-i LTA, MCM-22 and Al-MCM-41, only the acid sites on the external surface can be utilized in the catalytic reactions. A distinct difference in the product selectivity was also observed for the microporous and mesoporous catalysts.

Introduction

Zeolites are crystalline inorganic porous materials formed by TO_4 tetrahedra (T = Si, Al, P, *etc.*) with ordered microporous structures.[1] Because of their tunable acidities and framework structures, zeolites have been widely used in catalysis and molecular adsorption/separation as well as several other emerging applications.[1a, 2] However, the pore size of zeolite is usually smaller than 2 nm, which often causes severe diffusion limitation for the catalytic reactions involving bulky molecules. Introducing intracrystalline mesopores within zeolites forming hierarchical porous structures has proven to be a promising way to enhance the mass transport properties and catalytic performance of zeolite catalysts.[1b, 3]

Various synthesis approaches have been developed to fabricate mesoporous zeolites, such as exfoliating, or pillaring layered zeolites,[4] desilication or demetallation of zeolites by selective dissolution,[5] and soft and hard-templating methods.[6] Delaminated zeolites, such as ITQ-2, resulting from the delamination of a layered zeolite precursor, MCM-22(P), exhibit thin zeolite sheets (~2.5 nm thick) with a high external surface area (>700 m^2 g^{-1}).[4b] However, this method is only applicable for the materials composed of layered zeolite precursors. Using soft-templating synthesis strategy mesopores can be successfully introduced into zeolite crystals through the coherent assembly of zeolite precursors and specially designed structure directing agents (SDAs). Ryoo and co-workers have designed a series of diquaternary ammonium-type surfactants with long hydrophobic hydrocarbon chains to synthesize zeolites with ultrathin nanosheets.[4a, 6a, 7] Tsapatsis and co-workers have also reported one-step synthesis of self-pillared pentasil (SPP) zeolite composed of orthogonally connected single-unit cell lamellae.[8] 3 dimensionally ordered mesoporous imprinted (3DOm-i) zeolites synthesized using 3DOm carbon as a mesoscale hard template are hierarchical zeolites synthesized using a hard-templating synthesis strategy.[6b, 9]

Hierarchical zeolites with intracrystalline mesopores can provide easy access to the active sites located within micropores and fast mass transport which can improve the activity, selectivity and life time of zeolite catalysts for a wide range of catalytic reactions.[10] Although a series of breakthroughs have demonstrated the enhanced catalytic properties of hierarchical zeolites, the structure-property relationship for hierarchical zeolites has not been fully established yet.[1b, 11] There are several critical issues limiting the rational development of these materials for catalytic reactions. These include (1) the lack of facile methods for the synthesis of hierarchical zeolites with accessible and controllable mesopores; (2) the elusive contribution from the active sites on the external surface of hierarchical zeolites; (3) and the unclear mass transport behavior of hierarchical zeolites and their influences on catalyst performances.

Among these hierarchical zeolites synthesized by different approaches, 3DOm-i zeolites are ideal model materials for developing a fundamental understanding of the differences in catalytic activities of active sites in hierarchical zeolites because of their highly ordered and tunable mesoporous structures, framework compositions and a wide range of available framework

[a] *Dr. C. Li, Dr. Y. Ren, Prof. H. Xi*
School of Chemistry and Chemical Engineering
South China University of Technology
No. 381 Wushan Road, Guangzhou 510640 (China)
E-mail: cehxxi@scut.edu.cn

[b] *Dr. C. Li, Dr. H. J. Cho, Dr. Z. Wang, Prof. J. Gou, Prof. W. Fan*
Department of Chemical Engineering
University of Massachusetts, Amherst
159 Goessmann Lab, 686 North Pleasant Street, Amherst MA, 01003-9303 (USA)
Email: wfan@ecs.umass.edu

[c] *Dr. Z. Wang*
Department of Chemistry, College of Sciences
Northeastern University
No.3-11, Culture Road, Shenyang, Liaoning 110819 (China)

[d] *Prof. J. Gou*
College of Material Science and Technology
Beijing Forestry University
No.35 Tsinghua East Road, Beijing 100083 (China)

Supporting information for this article is available on the WWW under http://dx.doi.org/10.1002/cctc.xxxxxxxxx.

structures. In this study, we evaluated the accessibility and catalytic activities of a series of 3DOm-i zeolites with different topologies (*e.g.* MFI, LTA and BEA), and compared them to other conventional zeolites with a high external surface area such as MWW zeolite (MCM-22 and ITQ-2) and MFI nanocrystals. Amorphous mesoporous Al-MCM-41 material was also used in this study. The catalytic properties of Brønsted acid sites on the external and internal surface of these catalysts were investigated by liquid phase catalytic conversion of benzyl alcohol in mesitylene. The hierarchical zeolite catalysts exhibited enhanced catalytic performance and significant difference in product selectivity which is controlled by both mesoporosity and microporosity.

Results and Discussion

Structural properties of the catalysts

Zeolite catalysts studied in this work include small, medium and large micropore zeolites. Table 1 summarizes the topologies and pore systems of zeolite catalysts used in this study. LTA, a typical small pore zeolite, is built by connecting sodalite cages with double 4-membered rings (D4R), which creates *α* cage accessible *via* 8-membered rings (8 MR). MFI zeolite possesses an anisotropic framework with two intersecting 10-membered ring (10 MR) channels. The straight channel is parallel to the *b* axis, and the zigzag channel with an estimated pore opening of 0.51 nm × 0.55 nm is parallel to the *a* axis. The two channels along the *b* and *a* directions are interconnected, forming 3 dimensionally interconnected microporous structures. BEA is a large pore zeolite exhibiting 12-membered rings (12 MR), and is composed of an intersection of 0.77 nm × 0.66 nm and a tortuous channel of 0.56 nm × 0.56 nm. MCM-22 has an MWW framework structure which possesses a unique pore structure of 12 MR side cups on the crystal exterior, two independent 10 MR channel systems along the *a* and *b* axes and ultra-small 6-membered ring (6 MR) transport limiting apertures along the *c* axis. ITQ-2 is a 2 dimensional (2D) zeolite made from the delamination of MCM-22 precursors with 12 MR side "cups" on the external surface of the 2D sheets (~2.5 nm thick), these cups have an aperture of about 0.7 nm, which meet at the center of the sheets and connected with a double 6 MR window. As a result, ITQ-2 has a high external surface area (>700 m^2 g^{-1}) and affords reactants nearly unrestricted access to the acid sites on the surface.[4b, 12]

Table 1. Topologies and pore systems of zeolite catalysts.

Catalysts	Framework	Pore structure	
		Pore shape	Pore size (Å)
3DOm-i MFI	MFI	10 MR	5.1 × 5.5, 5.3 × 5.6 [a]
3DOm-i LTA	LTA	8 MR	4.1 × 4.1[a]
3DOm-i BEA	BEA	12 MR	7.7 × 6.6, 5.6 × 5.6 [b]
MCM-22	MWW	10 MR	4.0 × 5.5, 4.1 × 5.1 [a]
300 nm MFI	MFI	10 MR	5.1 × 5.5, 5.3 × 5.6 [a]
ITQ-2	N.A.	10 MR	4.1 × 5.1 [a]
Al-MCM-41	Amorphous	Hexagonal mesopores	*ca.*40 [c]

[a] Meier, W. M.; Olson, D. H. Zeolites 1992, 12, special issue Atlas of Zeolites Structure Type. [b] Ch. Baerlocher; L.B. McCusker; D.H. Olson. Atlas of Zeolite framework types (sixth edition). [c] Obtained from N_2 physisorption isotherms based on NLDFT method.

Aluminosilicate MCM-41(Al-MCM-41) is a mesoporous material from the M41S family with a hexagonal mesopore structure.

Figure 1a and Figure S1 show the wide-angle powder XRD patterns of zeolite catalysts used in this study. These patterns exhibit typical diffraction peaks for MFI, LTA, BEA, MCM-22 and ITQ-2 structures, consistent with previous reports.[4b, 6b, 9] Broad diffraction peaks were observed for 3DOm-i BEA sample, which is due to the highly intergrown zeolite BEA structure composed of different polymorphs. The small-angle XRD patterns of 3DOm-i zeolites are shown in Figure 1b, exhibiting well-resolved characteristic reflections for typical mesostructural ordering. This result implies that the 3DOm-i catalysts retain a high degree of 3 dimensionally ordered mesoporous ordering imprinted from the 3DOm carbon. According to a face-centered-cubic (FCC) structure, the diffraction peaks at low angle were indexed. The center-to-center distance between spherical elements calculated from the peak of (111) is 40 ± 5 nm which is in agreement with the pore size of the 3DOm carbon template and the TEM images shown in Figure 2. In addition, the diffraction peaks at low angle show a minor difference in the three 3DOm-i zeolites, which is most likely due to the small variation in the structures of the 3DOm carbon templates synthesized from different batches. MFI nanocrystal (300 nm MFI) has a similar XRD to 3DOm-i MFI, as shown in Figure 1a. ITQ-2 was made from the delamination of MCM-22 precursors. The absence of diffraction peaks from (001) and (002) planes in the XRD pattern of ITQ-2 clearly indicates that MCM-22 precursors have been delaminated (Figure S1 a).

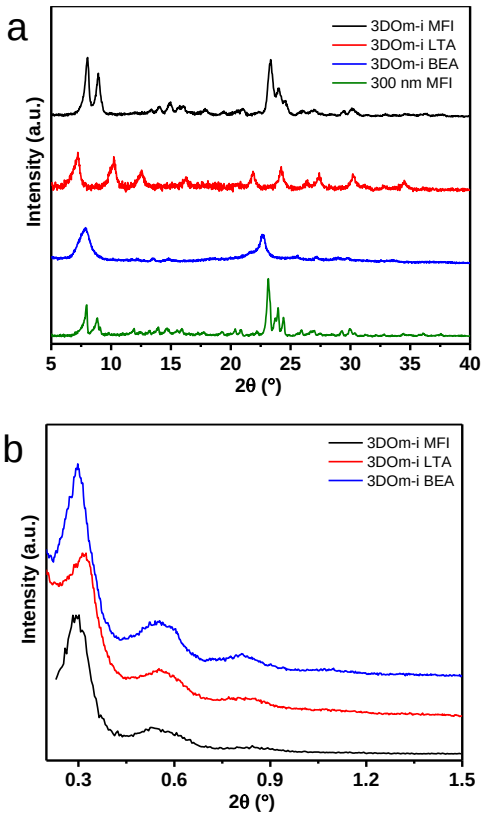

Figure 1. Crystalline structure of zeolite catalysts. a) Wide-angle XRD patterns of 3DOm-i MFI, 3DOm-i LTA, 3DOm-i BEA and 300 nm MFI, and b) Small-angle XRD patterns of 3DOm-i MFI, 3DOm-i LTA and 3DOm-i BEA.

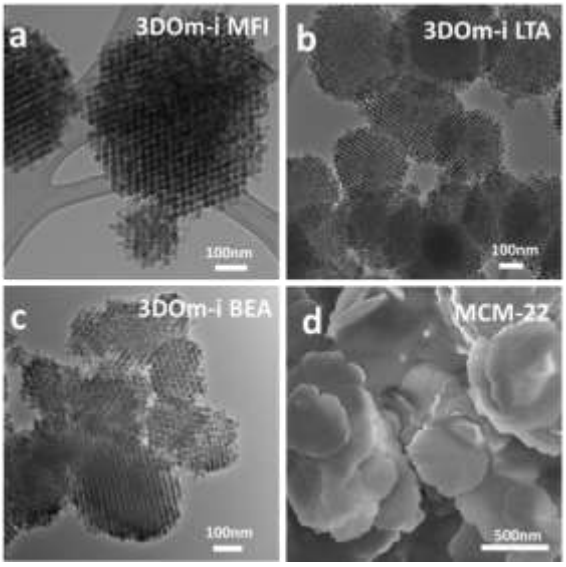

Figure 2. Morphologies of zeolite catalysts. TEM images of a) 3DOm-i MFI, b) 3DOm-i LTA and c) 3DOm-i BEA, and d) SEM image of MCM-22.

[4c, 13] Compared to the XRD pattern of MCM-22, ITQ-2 exhibits much broader peaks at high angle, consistent with the fact that MCM-22 precursors was delaminated into two dimensional nanosheet structures. The XRD of the Al-MCM-41 sample suggests that the sample possesses a hexagonal mesoporous structure (Figure S1 b).

N_2 physisorption isotherms at 77 K in Figure 3 show a sharp increase in the relative pressure range (P/P_0) from 0.6 to 0.8 in the adsorption branch and a clear hysteresis due to capillary condensation, confirming the presence of mesopores in the 3DOm-i catalysts. Mesopore size distributions calculated from the adsorption branch of the isotherms using None Localized Density Functional Theory (NLDFT) method indicate that the pore size is centered from 6 nm to 9 nm with a narrow pore size distribution (Figure S3). The textural characteristics of the catalysts including BET specific surface area, external surface area, micropore volume and total pore volume are summarized in Table 2. The BET specific surface areas (S_{BET}) of the 3DOm-i zeolite MFI, LTA and BEA are 477, 531 and 653 $m^2\ g^{-1}$, respectively. The external

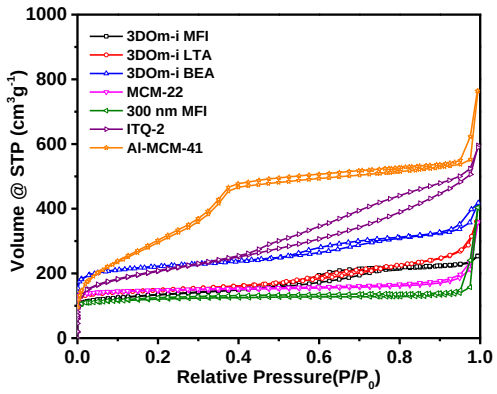

Figure 3. N_2 physisorption isotherms of zeolite catalysts.

Table 2. Textural properties of the zeolite catalysts determined by N_2 adsorption/desorption.

Catalyst	S_{BET} [$m^2\ g^{-1}$]	S_{ext} [a] [$m^2\ g^{-1}$]	V_{mic} [a] [$cm^3\ g^{-1}$]	V_{total} [b] [$cm^3\ g^{-1}$]
3DOm-i MFI	477	230	0.14	0.43
3DOm-i LTA	531	228	0.15	0.48
3DOm-i BEA	653	254	0.19	0.50
MCM-22	432	66	0.19	0.31
300 nm MFI	438	134	0.13	0.28
ITQ-2	674	345	0.20	0.50
Al-MCM-41	824	22	N.A.	0.78

[a] Calculated using *t*-plot method. [b] Calculated from the adsorption branch at P/P_0=0.95.

surface area (S_{ext}) ranges from 228 to 254 $m^2\ g^{-1}$, indicating that a large external surface area is created in the hierarchical zeolites. The micropore volumes calculated from *t*-plot method are 0.14, 0.15 and 0.19 $cm^3\ g^{-1}$, respectively, implying a high crystallinity for the 3DOm-i zeolite catalysts. On the other hand, MCM-22 only shows characteristic micropore filling ($P/P_0 < 0.05$) without any feature of mesoporosity. ITQ-2 sample shows a similar microporosity to MCM-22, but significant larger mesopore volume and external surface area (Table 2), which again indicates the micropore structure of ITQ-2 was well retained during the delamination process. The external surface area of MCM-22 is 66 $m^2\ g^{-1}$ which is much smaller than that of 3DOm-i zeolites. Based on the results, it can be concluded that all the 3DOm-i samples have both highly crystalline microporous structures associated with zeolite domains and mesoporous structures inherited from the 3DOm carbon template. However, MCM-22 sample mainly exhibits microporous structures because of the condensation of the layered MCM-22 precursors during the calcination.[4b, 4c]

Acid site distribution

The distribution of Brønsted acid sites in the hierarchical zeolites was investigated by temperature-programmed desorption (TPD) measurements. Isopropyl amine (IPA), 2,4,6-collidine (CLD) and triphenylphosphine (TPP) with different molecular sizes served as probe molecules to access the total acid sites (IPA-TPD) and acid sites on external surface of the zeolite catalysts (CLD-TPD or TPP-TPD), respectively.

IPA-TPD was used to determine the total number of Brønsted acid sites in each catalyst, as supported by the fact that adsorption occurs with 1:1 stoichiometry of IPA over the Brønsted acid sites in zeolite catalysts.[14] Table 3 shows the Si/Al ratio and Al concentration of the zeolite catalysts determined by elemental analysis (ICP-OES). The number of accessible Brønsted acid sites obtained from the IPA-TPD experiments is similar to the amount of Al in 3DOm-i ZSM-5, indicating that most of Al atoms are incorporated within the framework of these zeolite catalysts leading to Brønsted acidity. This result is consistent with the FT-IR measurement using pyridine as the probe molecule (Figure S5). 3DOm-i BEA and MCM-22 show lower Brønsted acid concentration than the amount of Al in the zeolites, indicating the presence of extra-framework Al in the zeolite sample. Interestingly, the total Brønsted acid sites in 3DOm-i LTA measured from the IPA-TPD measurement is significantly lower than the amount of Al in this sample. This is because IPA cannot

Table 3. Acid site distribution in the microporous and mesoporous catalysts.

Catalyst	Si/Al	Acid concentration (mmol g^{-1})			$f_{B,ext}$ [d] (Actual)	$f_{B,ext}$ [e] (Theoretical)
		Total [a] (Theoretical)	Total [b]	External surface [c]		
3DOm-i MFI	151	0.110	0.113	0.016	14.2 %	9.6 %
3DOm-i LTA	2.2	5.208	0.140	0.140	100 %	6.5 %
3DOm-i BEA	34	0.476	0.370	0.037	10.0 %	9.4 %
MCM-22	45	0.362	0.346	0.022	6.4 %	9.8 %
300 nm MFI	48	0.340	0.338	0.015	2.4 %	7.3 %
ITQ-2	50	0.327	0.325	0.179	55.1 %	100 %
Al-MCM-41	204	0.407	0.081	N.A.	N.A.	N.A.

[a] The number of total Brønsted acid sites calculated based on Si/Al ratio. [b] The number of total Brønsted acid sites determined by IPA-TPD. [c] The number of external Brønsted acid sites determined from CLD-TPD for 3DOm-i MFI, 3DOm-i LTA, MCM-22 and ITQ-2, and TPP-TPD for 3DOm-i BEA. [d] The fraction of external Brønsted acid sites calculated by (number of Brønsted acid sites by CLD-TPD or TPP-TPD / number of Brønsted acid sites by IPA-TPD). For 3DOm-i LTA, Brønsted acid sites detected by IPA are assigned to the acid sites on the external surface. [e] Calculated based on crystal shape and size and assuming a random distribution of Brønsted acid sites.

diffuse into the 8 MR in LTA structure and access the acid sites located on the internal surface at the adsorption temperature, 393 K. The observation is consistent with the previous study reported by Gorte *et al*.[14b] The acid site concentration for 3DOm-i LTA reported in Table 3 is, thus, only related to the accessible acid sites on the external surface of the catalyst.

In order to evaluate the acid sites on the external surface of the zeolite samples, a bulky amine molecule, 2,4,6-collidine (CLD), was used for 3DOm-i MFI, MCM-22 and ITQ-2 in the TPD measurements.[15] Since CLD with a kinetic diameter around 0.74 nm can easily diffuse into BEA micropores,[16] an even larger base molecule, triphenylphosphine (TPP), was used for 3DOm-i BEA. The acid site concentration on the external surface and ratio of external acid sites to the total acid site measured by CLD-TPD or TPP-TPD are listed in Table 3. The fraction of external Brønsted acid sites accessible to the bulky base molecules in 3DOm-i MFI and 3DOm-i BEA is 14.2% and 10.1%, respectively, which is about 2 times higher than that of MCM-22 (6.4%). The higher distribution of the Brønsted acid sites on the external surface of the 3DOm-i zeolites is mainly due to the hierarchical structures of zeolite catalysts. The fraction of external Brønsted acid sites accessible to CLD on ITQ-2 (55.1%) is much larger than MCM-22, because of the delaminated structure of ITQ-2. The values are also consistent with the theoretical values calculated based on crystal morphologies and an assumption of a random distribution of Brønsted acid sites. The results clearly support that the hierarchical structures created by the hard-templating method and delamination method can significantly improve the acid site distributions on the external surface of the zeolite catalysts.

Catalytic activity

3DOm-i zeolites with imprinted mesoporous structures and a large number of accessible Brønsted acid sites exhibit remarkable benefits for the catalytic reactions where diffusion constraints and/or adsorption of reactant molecules onto the active acid sites are main concerns. In this study, the liquid phase catalytic conversion of benzyl alcohol in mesitylene was used to evaluate the catalytic performance of the hierarchical zeolite catalysts.

Previous studies showed that two parallel reactions, self-etherification of benzyl alcohol and alkylation of mesitylene with benzyl alcohol, can be catalyzed by the Brønsted acid sites of zeolite catalysts.[8, 17] The products of the two reactions are dibenzyl ether (DE) and 1, 3, 5-trimethyl-2-benzylbenzene (TMBB), respectively, as shown in Scheme 1. It has been revealed that the alkylation of mesitylene with benzyl alcohol is exclusively catalyzed by the acid sites on the external surface of MFI zeolites because of the steric resistance of the bulky reactant and product, mesitylene and TMBB. Poisoning the external surface of the MFI zeolite catalysts with bulky amines such as 2,6-di-tert-butylpyridine (DTBP) can completely eliminate the production of TMBB. On the other hand, the production of DE from the self-etherification of benzyl alcohol can be catalyzed by the acid sites locatied on both the external and the internal surface of MFI zeolite catalysts. Due to the relatively large molecular size of benzyl alcohol, diffusion constraints have been observed for the reaction in MFI zeolites, and a diffusion-reaction model has been developed to interpret the reaction results.[17a, 18] Studying the liquid phase conversion of benzyl alcohol in mesitylene over the hierarchical zeolite catalysts provides critical insights into the catalytic activity and selectivity of the hierarchical zeolite catalysts.

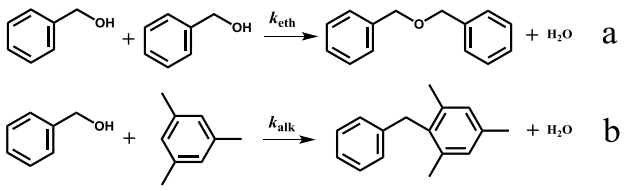

Scheme 1. Two reaction pathways of benzyl alcohol in mesitylene, a) benzyl alcohol self-etherification and b) alkylation of mesitylene with benzyl alcohol.

In this study, the conversion of benzyl alcohol in mesitylene over various zeolite catalysts was carried out to evaluate the effects of mesoporous and microporous structures on the catalytic performance. Figure 4 shows the conversions of benzyl alcohol in mesitylene over various zeolite catalysts at 343 K. Without poisoning the acid sites on the external surface, 3DOm-i BEA showed the highest conversion of benzyl alcohol than other 3DOm-i zeolite catalysts because the large 12 MR structure and mesoporous structure led to enhanced mass transport for the bulky reactants and products (Figure 4a). ITQ-2 and Al-MCM-41 also exhibited a high conversion due to the ease of access of acid sites located on the external surface. As expected, 3DOm-i MFI exhibited higher conversions than 300 nm MFI due to the imprinted mesoporous structures. 3DOm-i LTA and MCM-22 can also catalyze the reaction, but with much lower conversions, mainly because of their small microporous structures that limit the reaction exclusively occurring on the external surface of the catalysts. These results suggest that the presence of mesopores and large micropores (*e.g.* 12 MR) can significantly reduce the diffusion limitation in the alkylation of mesitylene with benzyl

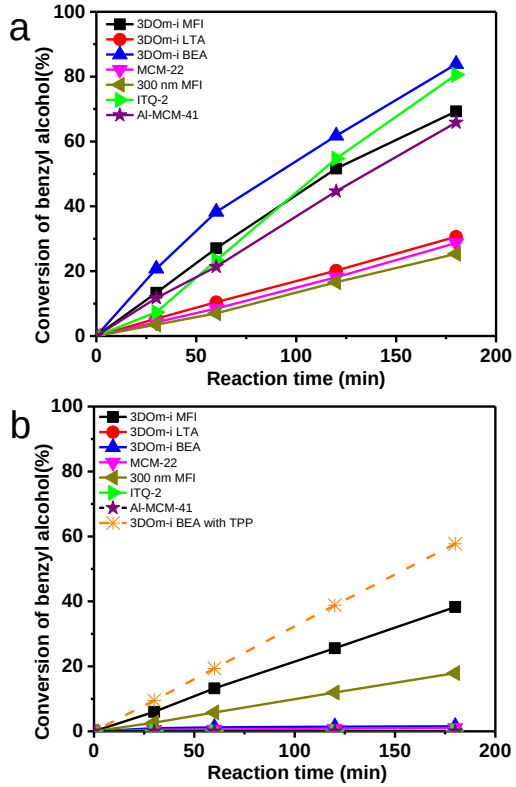

Figure 4. Catalytic conversions of benzyl alcohol in mesitylene over various zeolite catalysts. a) Mesitylene alkylation with benzyl alcohol (without DTBP) and b) benzyl alcohol self-etherification (with DTBP or TPP).

alcohol and etherification of benzyl alcohol. For this reason, 3DOm-i BEA catalyst exhibited superior catalytic performances for the reactions.

In contrast to mesoporous Al-MCM-41, the hierarchical zeolites with different microporosities offer an additional parameter to control the product selectivity in the reactions. The selectivities to TMBB and DE were calculated when the benzyl alcohol conversion was below 10 % (Table 4). Remarkably, a distinct difference in the product selectivity was observed between the zeolite catalysts and mesoporous Al-MCM-41. For 3DOm-i BEA and 3DOm-i MFI, the main product was DE from the etherification reaction, whereas the alkylated product, TMBB, was predominant for 3DOm-i LTA, MCM-22, ITQ-2 and Al-MCM-41. The difference in product selectivity arises from the small pore structure of 3DOm-i LTA, MCM-22 and ITQ-2 which limited most reactions occurring on the external surface favoring the formation of alkylated product. In addition, the external surface structure and terminal group concentration of the four zeolites are also largely different, which might also lead to different product selectivity as proposed in previous literature.[11b, 19]

The product selectivity can be further controlled by selectively tailoring the reactions over the external surface or internal surface of the hierarchical zeolites. It has been reported that poisoning the acid sites on the external surface of zeolite catalysts with bulky base molecules can completely prevent the formation of alkylated product in the reactions.[8] As shown in Figure 4b, in the presence of DTBP the conversion of benzyl alcohol was significantly decreased for 3DOm-i MFI, and almost completely eliminated for 3DOm-i BEA, 3DOm-i LTA, MCM-22, ITQ-2 and Al-MCM-41. The detectable product from 3DOm-i MFI catalyst was DE only. No alkylated product, TMBB, was observed in the reaction. The results clearly suggest that alkylated product was catalyzed by the acid sites on the external surface of the zeolite catalysts. Formation of DE can be catalyzed by the acid sites on the external and internal surface of MFI zeolite simultaneously. However, because of the small pore size of LTA and MCM-22, the acid sites on the internal surface cannot be utilized for the DE production. Surprisingly, the catalytic activity of 3DOm-i BEA was also almost completely prohibited in the presence of DTBP. This is likely because DTBP can poison the acid sites on both the external and internal surface of the large pore zeolite. In order to confirm the observation, instead of DTBP, TPP was added in the reaction to selectively poison the acid sites on the external surface of BEA zeolite. As expected, TPP exclusively adsorbed on the external surface of 3DOm-i BEA, leading to a much higher conversion of benzyl alcohol than the case of DTBP. A single product (DE) was observed in the reaction in the presence of TPP, which supports that the 12 MR in BEA zeolite cannot allow the formation of alkylated products in their micropores although the pore size is larger than that of MFI. The results clearly show the unique catalytic activity of hierarchical zeolites for selective production of DE from the self-etherification reaction. 3DOm-i BEA achieved the highest conversion of benzyl alcohol to DE on poisoning the acid sites on the external surface due to the 12 MR structure and interconnected mesopores. 3DOm-i MFI also selectively produced DE over the acid sites located within the zeolite, but with lower activity due to diffusion limitation compared to 3DOm-i BEA (10 MR *vs*. 12 MR). Neither small pore zeolites (*e.g.* LTA) nor mesoporous Al-MCM-41 can selectively produce DE from the reaction, due to the lack of control of acid site distributions for exclusive access by benzyl alcohol.

Table 4. Catalytic performance of the microporous and mesoporous catalysts for liquid phase catalytic reactions of benzyl alcohol in mesitylene.

Catalysts	Reaction rate constant [a]			Selectivity ($\alpha = 2C_E/C_C$)
	Alkylation (without DTBP)	Self-etherification (with DTBP)		
	$k_{alk,ext}$ [b] ($10^{-3}\cdot s^{-1}$[mol H^+]$^{-1}$)	$k_{alk,\ int}$ [c] ($10^{-6}\cdot L\cdot s^{-1}$[mol H^+]$^{-1}$)	$k_{eth,\ app,\ int}$ [c] ($10^{-6}\cdot L\cdot s^{-1}$[mol H^+]$^{-1}$)	
3DOm-i MFI	934.1	0	764.9	5.3
3DOm-i LTA	722.3	0	0	0.4
3DOm-i BEA	1882.0	0	0	6.4
3DOm-i BEA [d]	N.A.	0	2140.9 [d]	N.A.
MCM-22	9663.3	0	0	0.7
300 nm MFI	634.9	0	94.7	12.2
ITQ-2	6526.8	0	0	0.6
Al-MCM-41	1543.2	0	0	0.3

[a] Rate parameters determined by least-squares regression. [b] Normalized to number of external Brønsted acid sites determined by CLD-TPD or TPP-TPD measurement. [c] Normalized to number of internal Brønsted acid sites (internal acid sites = total acid sites - external acid sites). [d] This reaction data is calculated when TPP was added in the reaction.

In order to evaluate the catalytic activity of the acid sites within the hierarchical zeolites, the reaction rate constants for the conversion of benzyl alcohol in mesitylene over the external and internal surface of the hierarchical zeolites were calculated. The conversion data obtained with and without adding bulky base molecules were fitted well to a pseudo-first-order reaction model shown in SI. This allows us to determine the alkylation reaction and etherification reaction rate constants, respectively. First, the alkylation reaction rate constant, $k_{alk,ext}$, was calculated from the experimental data using Equation S7 and shown in Table 4 and Figure 5. Although the alkylation reaction only occurred on the external surface, the rate constant largely varied with the zeolite structures. Interestingly, the difference was as large as one order of magnitude from 0.634 s^{-1} to 9.663 s^{-1} with MCM-22 as the highest one and 300 nm MFI as the lowest one. The results suggest that it is possible to tailor the catalytic activity of zeolite catalysts by fabricating their external surface properties. It has been known that several parameters including adsorption properties, acid strength, steric constraints and Al distribution can affect the catalytic activity of the zeolite catalysts. In particular, for the alkylation reaction on the external surface, the unknown acid site distribution, terminal structure and defects in the structure can prevent the reaction rate constant from being directly associated with one single parameter of the zeolite catalysts. Therefore, based on the reaction results it cannot be concluded if the acid site strength of a certain zeolite is distinctly different from the others.

The self-etherification reaction rate constants within the micropores of different hierarhical zeolites are shown in Figure 6 and Table 4. 3DOm-i BEA exhibited the highest rate constant due to the enhanced mass transport and the large 12 MR structure. 3DOm-i MFI exhibited a lower rate constant than 3DOm-i BEA, but a higher value than 300 nm MFI, indicating the presence of diffusion constraints in MFI zeolites. The rate constants of 3DOm-i LTA, MCM-22, ITQ-2 and Al-MCM-41 are close to zero because DTBP can completely block the accessible acid sites for the self-etherification reaction. According to the same reason, so does the 3DOm-i BEA in the presence of TPP. The reaction rate constant for 3DOm-i BEA is similar to the one for self-pillared pentasil (SPP) zeolite with a diffusion length of only *ca.* 2 nm where the diffusion limitation was not observed. The similar reaction rate constant suggests that the self-etherification of benzyl alcohol in the 3DOm-i BEA is not constrained by diffusion limitation. The intrinsic reaction rate of self-etherification in BEA and MFI zeolites should not be significantly different.

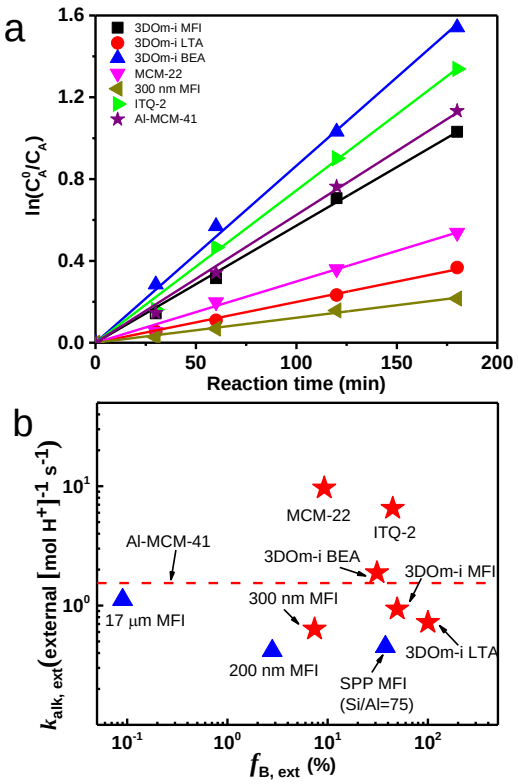

Figure 5. a) Plots for determination of rate constants of benzyl alcohol conversion in the absence of DTBP. (The selectivity over each catalysts can be found from Table 4. Reaction condition: total amount of catalysts used are ■3DOm-i MFI: 0.1 g, ●3DOm-i LTA: 0.2294 g, ▲3DOm-i BEA: 0.0692 g, ▼MCM-22: 0.0948 g, ◄300 nm MFI: 0.0970 g, ►ITQ-2: 0.1009 g, ★Al-MCM-41: 0.4049 g, respectively; The slope of each plot is the apparent rate constant, $k_{alk,app}$,). b) Reaction rate constant for mesitylene alkylation by benzyl alcohol ($k_{alk,\ ext}$) for various zeolite catalysts. (the data of 17 μm MFI, 200 nm MFI and SPP MFI (Si/Al=75) are from the ref.[8]

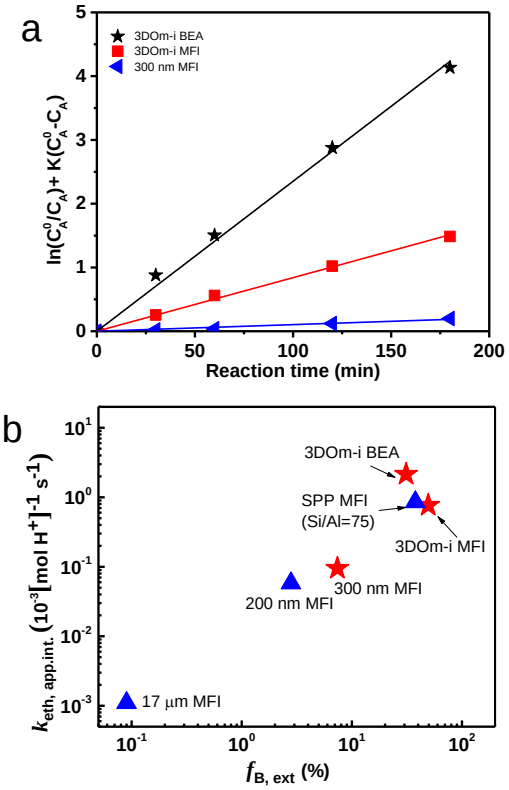

Figure 6. a) Plots for determination of apparent initial etherification rate constants of benzyl alcohol conversion inside the micropores in the presence of DTBP or TPP over different zeolite catalysts. (Reaction condition: total amount of catalysts used are ★3DOm-i BEA: 0.069 g, ■3DOm-i MFI: 0.1 g, ◄300 nm MFI: 0.097 g, respectively; (Slope of each plot is $k_{eth,app,int.}$ and can be determined from equation S2). b) Apparent internal self-etherification reaction rate constant ($k_{eth,\ app,\ int.}$) for various zeolite catalysts. (the data of 17 μm MFI, 200 nm MFI and SPP MFI (Si/Al=75) are from the ref.[8]

Conclusions

Hierarchical zeolites with ordered mesoporous structures and various frameworks were synthesized using a hard-templating method. The liquid phase catalytic reactions of benzyl alcohol in mesitylene was used as model reactions to evaluate catalytic activity of acid sites on both external and internal surface. Two parallel reactions occurred over these zeolite catalysts. It was observed that self-etherification of benzyl alcohol can be catalyzed by acid sites on both the external and internal surface of MFI and BEA zeolites. The 10 MR and 8 MR windows of MWW and LTA hinder the etherification reaction of benzyl alcohol. The alkylation of mesitylene with benzyl alcohol was exclusively catalyzed by the acid sites on the external surface of MFI, BEA, LTA, MCM-22, ITQ-2 and Al-MCM-41. It was found that the introduction of mesoporosity in zeolite structures can remarkably improve their catalytic performances by facilitating the accessibility of the acid sites within the micropores. After selectively poisoning the acid sites on the external surface by bulky base molecules, the catalytic activity of the acid sites on the internal surface of zeolite catalysts can be evaluated. Among the hierarchical zeolites, 3DOm-i BEA exhibited the highest activity for the etherification of benzyl alcohol, indicating that the large micropore and hierarchical structure can effectively reduce diffusion limitation for the reaction. Interestingly, without poisoning the acid sites on the external surface distinct product selectivity was achieved from the zeolite catalysts. Namely, 3DOm-i MFI, 3DOm-i BEA and 300 nm MFI prefer the etherification of benzyl alcohol, while 3DOm-i LTA, MCM-22, ITQ-2 and Al-MCM-41 favor the formation of alkylated product from benzyl alcohol and mesitylene. This is likely due to the different exteral surface structures of the zeolite catalsyts and the corresponding adsorption properties and acid strength. This study suggested that the liquid phase catalytic reactions of benzyl alcohol in mesitylene over hierarchical zeolite catalysts can proivde critical inisights into the catalytic performance of hierarchical zeolites. Futhermore, the presence of mesoporous structure and large external surface area on hierarchical zeolites not only enchance the catalytic activities, but also can change the selectivities of the zeolite catalysts.

Experimental Section

Catalysts Preparation

3DOm-i zeolites with MFI, BEA and LTA framework were synthesized according to the previous reports.[9, 20] Detailed synthesis procedure is available in supporting information. For comparison, MFI zeolite nano-crystals with a particle size of 300 nm, MWW zeolites (MCM-22 and ITQ-2) and mesoporous Al-MCM-41 were prepared according to the methods published in previous literature.[4b, 21] Ion-exchange of all catalysts were carried out with a 1 M aqueous solution of NH_4NO_3 at 353 K for 2 h and repeated three times. The final products were converted to proton form by calcination at 823 K for 8 h with a ramping rate of 1 K min^{-1} in a dry air flow.

Characterization

The X-ray diffraction (XRD) measurements were carried out on an X'pert Powder (PANalytical) diffractometer using a CuK_α radiation (λ = 0.15418 nm) with a Ni filter from 2θ of 4° to 40° with a step size of 0.04°. Small angle X-ray scattering (SAXS) patterns were collected on a Molecular Metrology SAXS line using a CuK_α radiation with a sample-to-detector distance of 1.48 m. Scanning electron microscopy (SEM) images were recorded on a FEI-Magellan 400 microscope, equipped with a field-emission gun operated at 3.0 kV. The samples were coated with Pt by sputtering at 60 mA for 60 s using Sputter Coater 208. Transmission electron microscopy (TEM) images were taken on a JEOL 2000FX microscope operated at 100 kV. The samples were first dispersed in ethanol with sonication, and then placed on a carbon-coated copper grid followed by evaporation at ambient conditions.

N_2 physisorption isotherms at 77 K were measured with a Quantachrome gas adsorption analyzer (Autosorb® iQ_2). Prior to the analysis, all catalysts were degassed at 573 K for 12 h. The specific surface area was calculated using the Brunauer-Emmett-Teller (BET) equation based on the adsorption branch curve obtained in a relative pressure (P/P_0) range of 0.05 - 0.3. The pore size distributions were obtained from the entire adsorption branch based on a non-localized density functional theory (NLDFT) method which describes N_2 adsorbed onto silica with cylindrical pores at 77 K (Versawin™ 1.0, Quantachrome).

Temperature-programmed desorption (TPD) measurements were performed on a thermogravimetric analysis instrument (TA® SDT Q600) to investigate the number of Brønsted acid sites of the catalysts following the method developed by Gorte *et al*..[14b, 22] Prior to the analyses, the catalysts (10.0 - 15.0 mg) were pretreated at 773 K for 1 h in a helium flow to clean the catalyst surface. After the samples cooled down to 393 K, an isopropylamine (IPA)/He gas mixture was passed through the sample at 100 mL min^{-1}. After the adsorption of IPA reaches to equilibrium onto the catalysts, the temperature was raised from 393 K to 1023 K with a ramping rate of 10 K min^{-1}. The decomposition of IPA into ammonia and propene on the Brønsted acid sites of zeolite catalysts occurring between 575 K and 650 K was used to calculate the total amount of Brønsted acid sites of the catalysts. 2,4,6-collidine (CLD) which is too bulky to diffuse into MFI micropores was used to quantify acid sites on the external surface of 3DOm-i ZSM-5[8] and MCM-22.[23] A typical CLD-TPD experiment was run on the same thermogravimetric analysis instrument as IPA-TPD, with exception of using CLD as the adsorbate. A larger basic molecule, triphenylphosphine (TPP), was used to evaluate the acid sites on the external surface of BEA zeolite as suggested by literature.[11b, 19c, 24] 3DOm-i BEA was first calcined at 823 K for 8 h in an air flow to remove the adsorbed impurities. 1 mL of CH_2Cl_2 solution containing 10^{-7} M of TPP was added into the calcined BEA zeolite. The sample was washed with an excess amount of CH_2Cl_2 to remove the weakly adsorbed TPP. Finally, the sample was dried in an oven at 393 K overnight to remove CH_2Cl_2. The subsequent procedure was the same as described above for IPA-TPD and CLD-TPD measurements. For the case of Al-MCM-41, IPA-TPD was used to measure the amount of acid sites on the surface.

Catalytic Reaction

Liquid phase catalytic conversion of benzyl alcohol in mesitylene was chosen as a model reaction to investigate the catalytic performance of 3DOm-i zeolites and other conventional zeolites with a large external surface area. The reaction was carried out in a three-necked round-bottom flask (100 mL) equipped with a reflux condenser under atmospheric pressure. The temperature of the reflux condenser was kept at 270 K. The flask was heated in a temperature controlled oil bath (343 K) with a magnetic stirring of 500 rpm. Prior to the reactions all catalysts were activated in a muffle furnace at 823 K for 4 h under a dry air flow (100 mL min^{-1}). Typically, 0.15 g of 3DOm-i BEA corresponding to 7.04×10^{-5} mol of Brønsted acid sites was added to the flask containing 15 mL of mesitylene (98%, Aldrich). The amount of 3DOm-i MFI, 3DOm-i LTA, MCM-22, ITQ-2 and Al-MCM-41 used in the reactions were adjusted to keep the amount of Brønsted acid in the reactor the same as the case of 3DOm-i BEA. The reaction mixture was maintained for 1 h at 343 K with stirring prior to the addition of 0.25 mL of benzyl alcohol (ACS reagent, ≥99.0%, Aldrich). Reaction time was defined as the moment when benzyl

alcohol was added. Samples were collected periodically and analyzed on a gas chromatograph (Agilent HP-6890 GC) equipped with a methylsiloxane capillary column (HP-1, 50.0 m × 20 μm × 0.52 μm) connected to a flame ionization detector.

According to previous studies, 2,6-di-tert-butylpyridine (DTBP, ≥97%, Aldrich) can be used to selectively poison the Brønsted acid sites on the external surface of zeolite catalysts with MFI and MWW structures without significantly changing the performance of the active sites located on the internal surface.[17a, 18] To study the reactions catalyzed only by the acid sites on the internal surface of the 3DOm-i zeolite catalysts, an excess amount of DTBP was added in the reactor (the moles of DTBP are 5 times higher than that of total acid from the zeolite catalysts) before the reaction. The mixture was then refluxed for 2.5 h at 343 K with stirring to make sure that DTBP was adsorbed on the acid sites located on the external surface of the zeolite catalysts. 0.25 mL of benzyl alcohol was then added into the mixture. In the case of 3DOm-i BEA, TPP was used to poison the external acid sites of 3DOm-i BEA since DTBP can diffuse into the micropores of BEA zeolites. Liquid samples were collected and analyzed using the same method described above. Blank test was also run under the same condition without adding catalysts. The result showed that there was no conversion of benzyl alcohol after 3 h in the absence of zeolite catalysts.

Acknowledgements

This work was supported by the Catalysis Center for Energy Innovation, an Energy Frontier Research Center funded by the US Dept. of Energy, Office of Science, and Office of Basic Energy Sciences under award number DE-SC0001004.

Keywords: 3DOm-i • hierarchical zeolite • diffusion limitation • self-etherification reaction • alkylation reaction

[1] a) A. Corma, *Chem. Rev.* **1997**, *97*, 2373-2420; b) J. Perez-Ramirez, C. H. Christensen, K. Egeblad, J. C. Groen, *Chem. Soc. Rev.* **2008**, *37*, 2530-2542; c) W. J. Roth, P. Nachtigall, R. E. Morris, J. Čejka, *Chem. Rev.* **2014**, *114*, 4807-4837.

[2] a) M. E. Davis, *Nature* **2002**, *417*, 813-821; b) B. Smit, T. L. M. Maesen, *Chem. Rev.* **2008**, *108*, 4125-4184.

[3] a) C. M. A. Parlett, K. Wilson, A. F. Lee, *Chem. Soc. Rev.* **2013**; b) K. Egeblad, C. H. Christensen, M. Kustova, C. H. Christensen, *Chem. Mater.* **2008**, *20*, 946-960; c) M. Hartmann, *Angew. Chem. Int. Ed.* **2004**, *43*, 5880-5882; d) Y. S. Tao, H. Kanoh, L. Abrams, K. Kaneko, *Chem. Rev.* **2006**, *106*, 896-910; e) J. Cejka, S. Mintova, *Catal. Rev.-Sci. Eng.* **2007**, *49*, 457-509.

[4] a) K. Na, M. Choi, W. Park, Y. Sakamoto, O. Terasaki, R. Ryoo, *J. Am. Chem. Soc.* **2010**, *132*, 4169-4177; b) A. Corma, V. Fornes, S. B. Pergher, T. L. M. Maesen, J. G. Buglass, *Nature* **1998**, *396*, 353-356; c) S. Maheshwari, E. Jordan, S. Kumar, F. S. Bates, R. L. Penn, D. F. Shantz, M. Tsapatsis, *J. Am. Chem. Soc.* **2008**, *130*, 1507-1516; d) I. Ogino, E. A. Eilertsen, S.-J. Hwang, T. Rea, D. Xie, X. Ouyang, S. I. Zones, A. Katz, *Chem. Mater.* **2013**, *25*, 1502-1509.

[5] J. C. Groen, J. Pérez-Ramírez, in *Novel Concepts in Catalysis and Chemical Reactors* (Eds.: A. Cybulski, J. A. Moulijn, A. Stankiewicz), Wiley-VCH, Weinheim, **2010**, pp. 31-50.

[6] a) M. Choi, K. Na, J. Kim, Y. Sakamoto, O. Terasaki, R. Ryoo, *Nature* **2009**, *461*, 246-249; b) W. Fan, M. A. Snyder, S. Kumar, P.-S. Lee, W. C. Yoo, A. V. McCormick, R. Lee Penn, A. Stein, M. Tsapatsis, *Nat. Mater.* **2008**, *7*, 984-991.

[7] K. Na, C. Jo, J. Kim, K. Cho, J. Jung, Y. Seo, R. J. Messinger, B. F. Chmelka, R. Ryoo, *Science* **2011**, *333*, 328-332.

[8] X. Zhang, D. Liu, D. Xu, S. Asahina, K. A. Cychosz, K. V. Agrawal, Y. Al Wahedi, A. Bhan, S. Al Hashimi, O. Terasaki, M. Thommes, M. Tsapatsis, *Science* **2012**, *336*, 1684-1687.

[9] H. Chen, J. Wydra, X. Zhang, P.-S. Lee, Z. Wang, W. Fan, M. Tsapatsis, *J. Am. Chem. Soc.* **2011**, *133*, 12390-12393.

[10] M. S. Holm, E. Taarning, K. Egeblad, C. H. Christensen, *Catal. Today* **2011**, *168*, 3-16.

[11] a) J.-C. Kim, K. Cho, R. Ryoo, *Appl. Catal. A* **2014**, *470*, 420-426; b) W. Kim, J.-C. Kim, J. Kim, Y. Seo, R. Ryoo, *ACS Catal.* **2013**, *3*, 192-195; c) K. Kim, R. Ryoo, H.-D. Jang, M. Choi, *J. Catal.* **2012**, *288*, 115-123.

[12] A. Corma, V. Fornés, J. M. Guil, S. Pergher, T. L. M. Maesen, J. G. Buglass, *Microporous Mesoporous Mater.* **2000**, *38*, 301-309.

[13] A. Corma, V. Fornes, J. Martinez-Triguero, S. B. Pergher, *J. Catal.* **1999**, *186*, 57-63.

[14] a) O. Kresnawahjuesa, R. J. Gorte, D. de Oliveira, L. Y. Lau, *Catal. Lett.* **2002**, *82*, 155-160; b) C. Pereira, R. J. Gorte, *Appl. Catal. A* **1992**, *90*, 145-157.

[15] a) M. Niwa, N. Katada, *Chem. Rec.* **2013**, *13*, 432-455; b) A. Corma, V. Fornés, L. Forni, F. Márquez, J. Martínez-Triguero, D. Moscotti, *J. Catal.* **1998**, *179*, 451-458.

[16] F. Thibault-Starzyk, I. Stan, S. Abelló, A. Bonilla, K. Thomas, C. Fernandez, J.-P. Gilson, J. Pérez-Ramírez, *J. Catal.* **2009**, *264*, 11-14.

[17] a) D. Liu, X. Zhang, A. Bhan, M. Tsapatsis, *Microporous Mesoporous Mater.* **2014**, *200*, 287-290; b) P. Sazama, B. Wichterlová, Š. Sklenák, V. I. Parvulescu, N. Candu, G. Sádovská, J. Dědeček, P. Klein, V. Pashkova, P. Šťastný, *J. Catal.* **2014**, *318*, 22-33.

[18] D. Liu, A. Bhan, M. Tsapatsis, S. Al Hashimi, *ACS Catal.* **2011**, *1*, 7-17.

[19] a) D. Liu, X. Zhang, A. Bhan, M. Tsapatsis, *Microporous Mesoporous Mater*; b) K. Góra-Marek, K. Tarach, M. Choi, *J. Phys. Chem. C* **2014**; c) H. Wei, K. Liu, S. Xie, W. Xin, X. Li, S. Liu, L. Xu, *J. Catal.* **2013**, *307*, 103-110.

[20] Z. Wang, P. Dornath, C.-C. Chang, H. Chen, W. Fan, *Microporous Mesoporous Mater.* **2013**, *181*, 8-16.

[21] a) H. Mochizuki, T. Yokoi, H. Imai, R. Watanabe, S. Namba, J. N. Kondo, T. Tatsumi, *Microporous Mesoporous Mater.* **2011**, *145*, 165-171; b) M. E. Leonowicz, J. A. Lawton, S. L. Lawton, M. K. Rubin, *Science* **1994**, *264*, 1910-1913; c) T. Applied Catalysis A: GeneralKugita, S. K. Jana, T. Owada, N. Hashimoto, M. Onaka, S. Namba, *Appl. Catal. A* **2003**, *245*, 353-362.

[22] a) J. G. Tittensor, R. J. Gorte, D. M. Chapman, *J. Catal.* **1992**, *138*, 714-720; b) R. J. Gorte, *J. Catal.* **1982**, *75*, 164-174.

[23] a) H. Du, D. H. Olson, *J. Phys. Chem. B* **2001**, *106*, 395-400; b) S. Inagaki, K. Kamino, E. Kikuchi, M. Matsukata, *Appl. Catal. A* **2007**, *318*, 22-27.

[24] a) W. P. Rothwell, W. X. Shen, J. H. Lunsford, *J. Am. Chem. Soc.* **1984**, *106*, 2452-2453; b) J.-H. Kim, A. Ishida, M. Niwa, *React. Kinet. Catal. Lett.* **1999**, *67*, 281-287; c) P. Andy, J. Garcia-Martinez, G. Lee, H. Gonzalez, C. W. Jones, M. E. Davis, *J. Catal.* **2000**, *192*, 215-223.

Entry for the Table of Contents

Layout 1:

FULL PAPER

The effects of frameworks and mesoporosities on the catalytic activity of hierarchical zeolite catalysts were investigated by studying the catalytic performance of 3 dimensionally ordered mesoporous imprinted (3DOm-i) zeolites and comparing them to other microporous and mesoporous catalysts with a high external surface area. It was found that the mesoporosity in MFI and BEA zeolites can effectively enhance the catalytic performance of the zeolite catalysts for the benzyl alcohol self-etherification catalyzed by both the acid sites on the external and internal surface, and the alkylation of mesitylene with benzyl alcohol exclusively catalyzed by the acid sites on the external surface.

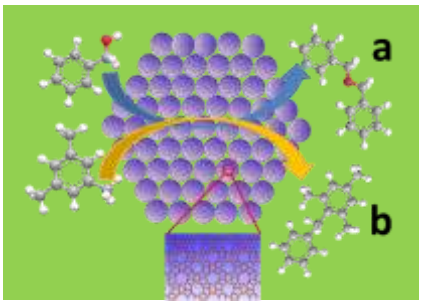

Chao Li, Hong Je Cho, Zhuopeng Wang, Jinsheng Gou, Yanqun Ren, Hongxia Xi, and Wei Fan**

Page No. – Page No.

Effects of Frameworks and Mesoporosities on the Catalytic Activity of Hierarchical Zeolite Catalysts in Benzyl Alcohol Conversion